

Modelling Phase Change in a
3D Thermal Transient Analysis

by

E.E.U. Haque, P.R. Hampson

reprinted from

**THE INTERNATIONAL JOURNAL OF
MULTIPHYSICS**

2014: VOLUME 8 NUMBER 1

MULTI-SCIENCE PUBLISHING

Modelling Phase Change in a 3D Thermal Transient Analysis

E.E.U. Haque, P.R. Hampson*

School of Computing, Science and Engineering
University of Salford
Salford, M5 4WT, UK

ABSTRACT

A 3D thermal transient analysis of a gap profiling technique which utilises phase change material (plasticine) is conducted in ANSYS. Phase change is modelled by assigning enthalpy of fusion over a wide temperature range based on Differential Scanning Calorimetry (DSC) results. Temperature dependent convection is approximated using Nusselt number correlations. A parametric study is conducted on the thermal contact conductance value between the profiling device (polymer) and adjacent (metal) surfaces. Initial temperatures are established using a linear extrapolation based on experimental data. Results yield good correlation with experimental data.

Key words: Transient thermal analysis, Phase change, Gap profiling

1. INTRODUCTION

Manufacture and assembly of structures is a complex process wherein the final stages of assembly gaps may be found between mating surfaces of components that are to be mechanically-fastened[1]. This fact is inherent in all manufacturing and assembly processes as the control over such processes are always finite[2], however the variations are reported to be larger in components manufactured using composites as opposed to traditional engineering alloys[3]. The gaps arise due to an individual component's manufacturing tolerances, which when placed in their respective final positions present significant deviations from their nominal dimensions due to the summation of the individual variations. These gap heights typically range from 0 to 2.5 mm.

The Gap Sachet (Figure 1) is a device created for the purpose of profiling gaps arising between mating faces of components and is intended for use in conjunction with one of the many 3D surface digitizing technologies for digital mapping[4]. The device works by injecting a moulding material, plasticine (in its liquid state), into a fabricated thin plastic film (nylon) retainer which is placed into the gap to be profiled. The injection is achieved by a heated motorised-extruder unit, having fixed mass flow rate and injection temperature. The plasticine within the Gap Sachet is allowed to cool and upon hardening it is removed providing a sectional profile of the gap.

This paper aims to model in ANSYS v11.0, the various transient thermal processes involved during the cooling of the Gap Sachet, including the phase change of plasticine and the effect of thermal contact conductance between a polymer-metal interface. The thermal effects taking place during the injection process is approximated and applied as a time dependent thermal load to describe the initial conditions. The results obtained are compared with experimental data.

* Corresponding author. Tel.; +44 (0) 161 295 4983; fax; +44 (0) 161 295 5575
E-mail address: p.r.hampson@salford.ac.uk

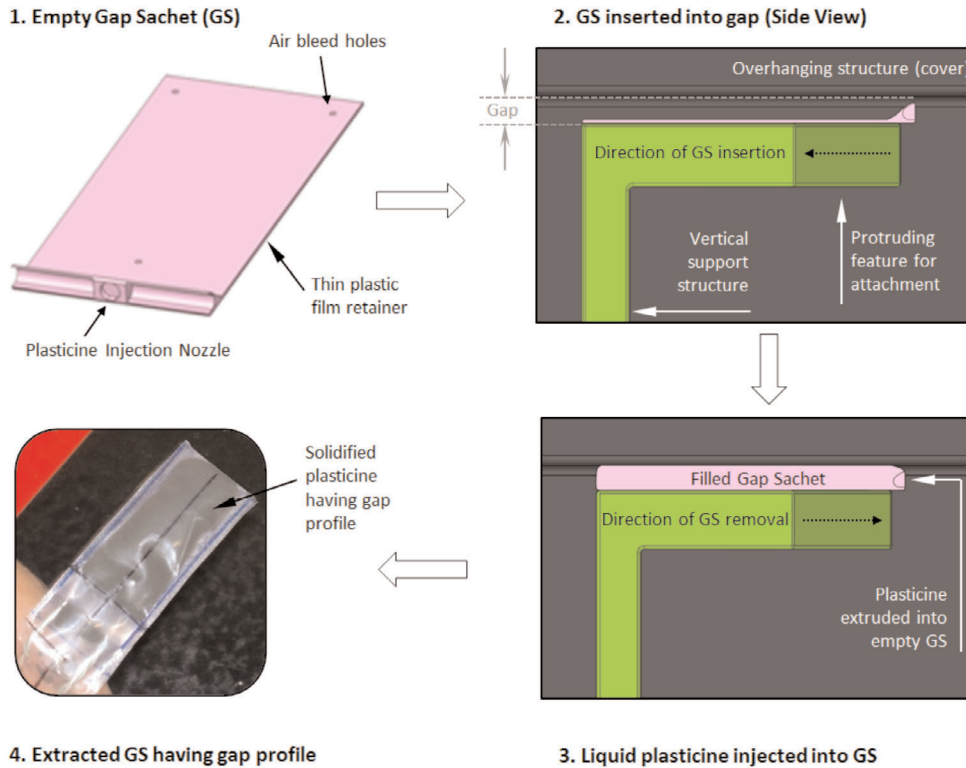


Figure 1: Gap sachet concept

2. PROBLEM SPECIFICATION & BOUNDARY CONDITIONS

The gap to be profiled may take on various shapes and sizes and are typically located between components that are required to be fastened; consisting of a wide overhead cover (Top Plate) which attaches onto a smaller structural support component (Bottom Plate) in order to maintain its shape. For the purpose of this paper, the gap in between the two components is assumed to have constant rectangular cross section and a height of 2.5 mm.

Figure 2 shows the front and top views of a filled Gap Sachet which has been placed into a typical idealised gap model, indicating the thermal processes involved during cooling. Four main bodies are established; (1) Plasticine (2) Plastic Film (3) Top Plate and (4) Bottom Plate, whose material properties are listed in Table 1.

The ideal placement of the Gap Sachet for gap profiling is along the centre line of the Top and Bottom Plates thus having geometrical symmetry along the z and x-axes, however it is assumed to have thermal symmetry only along the z-axis (axes detailed in Figure 8). Therefore, only half the system is to be modelled.

The computational model of the Gap Sachet is assumed to encompass the entire gap within its designed volume (30 x 7.5 x 2.5 mm, length x width x height) and is defined as two components. A rectangular hollow block (thin film plastic, wall thickness 0.0508 mm) which surrounds a solid block (plasticine). The idealised Top and Bottom Plates have dimensions 50 x 25 x 6 mm and 30 x 15 x 6 mm respectively. Four measurements are made (T_1 , T_2 , Top & Bot) as indicated in Figure 2 whose positions are detailed in Table 2.

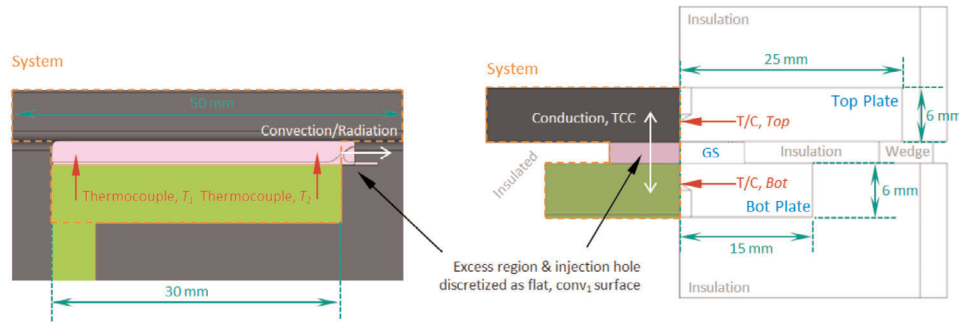


Figure 2: Computational model dimensions & boundary conditions

Table 1: Material thermal properties

Material	k [W/m-K]	C_p [J/kg]	ρ [kg/m ³]
Aluminium	180 [ref 56]	921 [ref 57]	2700 [ref 58]
Thin film nylon plastic	0.35 [ref 59]	1,700 [ref 59]	1,130 [ref 60]
Plasticine	0.65 [ref 36]	1,255	1608.46

Table 2: Co-ordinates of temperature readings for T_1 , T_2 , TOP and BOT for ANSYS & Experiment (axes detailed in Figure 8)

Reading	X [mm]	Y [mm]	Z [mm]
Top	0	11.5	15
Bot	0	3	15
T_1	0	7.25	3
T_2	0	7.25	27

Three modes of heat transfer are identified for the model: (1) Conduction (2) Convection and (3) Radiation. The rate of conduction is defined by the material properties for each respective body. Convection effects are computed by approximation of the fluid film coefficient with respect to surface and bulk fluid temperature, assuming natural convection. All faces are assumed to be insulated limiting the effects of convection being applied on the exposed face (henceforth referred to as the conv₁ face).

Also, the Top and Bottom Plates are also considered to be insulated on all sides except the region within which the Gap Sachet is to be inserted (Figures 2 and 3). For the experiment, due to the size of the insulation, combined with its overall dimensions a channel of depth 15mm exists perpendicular to the conv₁ face. However, as the insulating material does not produce any heat flux, it is assumed to play no role in the rate of transfer of heat from the exposed face. Further, the injection hole is not modelled in the simulation to reduce the computational costs of the analysis. The effects of radiation are assumed to be negligible.

As the plasticine is to be injected in its fluidic state into the Gap Sachet using the motorised-extruder, during cooling the plasticine mould solidifies taking the shape of the gap. Modelling of this phase change (liquid to solid) is the main aim of the computational analysis through application of an enthalpy based model which describes the energy released

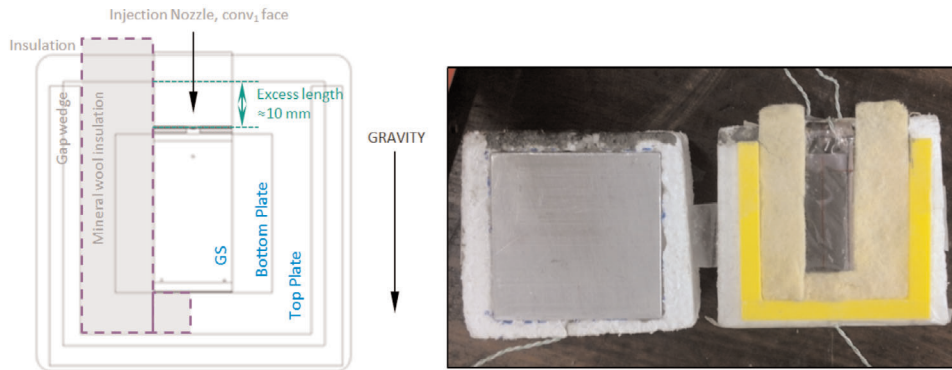


Figure 3: Experimental setup for verification

during cooling (latent heat of fusion). The model's accuracy is of interest in this paper and its application to plasticine will be studied.

It is well known that for surfaces in contact, perfect conduction is never achieved between the two bodies. A temperature discontinuity exists at the mating interface due to the micro-asperities on the surface of both components. The thermal contact conductance is a result of contact only being made at a select number of points, as opposed to the entire surface area of the bodies in contact[5].

One method of computationally obtaining the value of thermal contact conductance is based on curve-fitting of the experimental temperature readings (vs. time) at specific locations within a system with the computational results. This is achieved by varying the value of thermal contact conductance across a wide range until a good match is obtained[6]. While it is clear that experimental measurements of thermal contact conductance yield suitable results for specified parameters, the aforementioned indirect method is commonly used in conjunction with FEA packages where only the thermal loads are known[7]. A parametric study is conducted for the values of thermal contact conductance between the range 200 to 800 [W/ K] in steps of 200.

The motorised-extruder has fixed initial temperature ($T_{\text{Injection}} = 85$ [°C]) and constant mass flow rate of 1.326 [g/s], taking approximately 1.7 [s] to fill the Gap Sacht with plasticine. The flow of plasticine from the extruder into the Gap Sacht is not modelled. However, the temperature profile generated as a result of the flow into the Gap Sacht is approximated from experimental data and applied as initial conditions.

The profile is derived by linearly extrapolating temperature values at 2.5 mm intervals between thermocouple readings T_1 and T_2 (Figure 4) and applying them within quadrants in the computational model, assumed constant along the cross-sectional profile (x-axis). As the duration to fill the Gap Sacht is small in comparison to the overall length of the simulation, it is assumed that the effect of convection within the liquid plasticine is small and that conduction is the dominant heat transfer mode throughout the temperature range of plasticine.

Initial body temperatures are averaged and applied for the computational analyses. Temperature results are extracted from points T_1 , T_2 , Top & Bot and compared with experimental data.

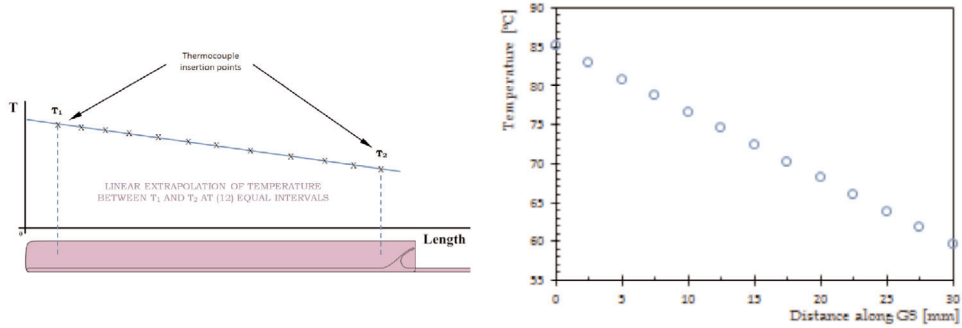


Figure 4: Initial temperature profile approximation

3. LITERATURE REVIEW

3.1 CONDUCTION

Two modes of heat transfer are considered in this analysis: Conduction and Convection. The governing equation for a non-linear 3D (Cartesian coordinate) transient heat conduction problem in ANSYS is given by consideration of the first law of thermodynamics as applied to a differential control volume yielding [8][9][10]:

$$\frac{\partial T}{\partial t} = \alpha \nabla^2 T + \frac{\dot{q}}{\rho c_p} \tag{1}$$

Where T [K] is the spatial (x, y, z) [m] and time (t) [s] dependent temperature, $\partial T/\partial t$ is the rate of change of temperature at a point with respect to time, \dot{q} [J/m³.s] is the internal heat generation rate per unit volume, ρ [kg/m³] is the density, c_p [J/kg-K] is the specific heat capacity at constant pressure and α is the thermal diffusivity [m²/s].

Using the Galerkin Weighted Residual Method[11] to integrate around the volume of an element (e), while taking into account the boundary conditions (spatial temporal dependence of temperature, convection and heat flow)[12] and substitution of the shape function of the elements[13], for FEA analysis in ANSYS [10], Eqn. (1) may be written in the following matrix form:

$$[C_e^t] \{\dot{T}_e\} + ([K_e^{tb}] + [K_e^{tc}]) \{T_e\} = \{Q_e^c\} \tag{2}$$

Where the subscript e signifies the matrix defining the respective element, $[C_e^t]$ is the element specific heat matrix [J/kg-K], $\{\dot{T}_e\}$ is the rate of change of temperature for each node [°C/s], $[K_e^{tb}]$ is the element diffusion conductivity matrix, $[K_e^{tc}]$ is the element convection surface conductivity matrix, $\{T_e\}$ is the temperature at the node, $\{Q_e^c\}$ is the element convection surface heat flow vector. Based on the initial parameters and material properties, the Newton-Raphson algorithm is employed in ANSYS to solve the discretised, non-linear equation for a set time at pre-defined intervals, solving for $\{Q_e^c\}$ [14].

3.2 CONVECTION

It is assumed the effects of convection are localised to the exposed surface of the Gap Sachet, having dimensions of $L = 0.015$ [m] and $W = 0.0025$ [m], where due to its orientation, it is idealised as a flat horizontal plate. In Eqn (2) the $[K_e^{tc}]$ and $\{Q_e^c\}$ matrices contain the surface heat transfer coefficient term (h_f) [W/m²-K], defined from Newton's Law of Cooling [15]:

$$q = h_f (T_B - T_S) \quad (3)$$

Where q is the heat flux per unit area [W/m²]. The coefficient is to be evaluated at $(T_B + T_S)/2$ (film temperature, T_f [°C]), where T_B [°C] is the Bulk Temperature measured at a distance for the surface and T_S [°C] is the temperature at the surface of the element.

Various methods exist to numerically estimate the value of h_f for the purpose of computational simulation. One common method is the application of the appropriate Nusselt number correlations to simulate the aid in cooling achieved through the exposed surface due to convection. The procedure involves establishing fluid properties for a range of working film temperatures and determining the corresponding convective parameters, allowing the computation of h_f [16][17] [18][19][20].

The fluid (air) properties are established within a working range of $T_\infty < T < 85$ [°C] using correlations developed for dry air at one atmosphere by Ref [21]. The Nusselt number (Nu) expresses the overall heat transfer phenomenon and is defined as the ratio of the convective heat flow to the heat transferred by conduction [17]:

$$Nu = \frac{h_f L^*}{k} \quad (4)$$

Where k [W/m-K] is the thermal conductivity of the fluid for the film temperature (T_f) being evaluated, h_f [W/m²-K] is the convective heat transfer coefficient, and L^* [m] is the characteristic length [22] [23] defined by:

$$L^* = \frac{A}{P} \quad (5)$$

Where A is the area [m²] and P is the perimeter [m]. The Nusselt number [17] is described by two dimensionless parameters of the form:

$$Nu = f(Gr^m \cdot Pr^n) \quad (6)$$

Where Gr is the Grashof number, the ratio of the buoyancy forces to viscous forces, Pr is the Prandtl number, the ratio of momentum and thermal diffusivities and m and n are exponents obtained from experiments. The Grashof number [16] is defined as:

$$Gr = \frac{g\beta(T_s - T_B)L^3}{\nu^2} \quad (7)$$

Where g is the acceleration due to gravity [m/s²], β [1/°K] is the thermal expansion

coefficient of the fluid and ν [m^2/s] is the kinematic viscosity of the fluid, both evaluated at the film temperature, T_f . The Prandtl number [24] is defined as:

$$\text{Pr} = \frac{c_p \mu}{k} \quad (8)$$

The product of Gr and Pr defines the dimensionless constant Ra, the Rayleigh number [16]:

$$\text{Ra} = \text{Gr} \cdot \text{Pr} \quad (9)$$

The Rayleigh number indicates the dominant heat transfer mechanism, whose value when below the order of 10^3 indicates dominant heat transfer through conduction, while an increasing value signifies the takeover of heat transfer by convection[25]. Empirical correlations between Nu and Ra for flat plates [16] are defined in the following form:

$$\text{Nu} = \text{C} \text{Ra}^{\frac{n}{m}} \quad (10)$$

Where the constants C, n and m are defined based on the range of Ra, values of which may be found in literature. The following Nusselt number correlation is used in order to compute the range of values of h_f : [26][23]

$$1 < \text{Ra} < 10^2 \quad \text{Nu} = 0.960(\text{Ra})^{1/6} \quad (\text{various shapes}) \quad (11)$$

Upon establishing the Nusselt number (Eqn. 11) based on flow parameters (Eqns. 7 to 9) that are derived based on film temperature (T_f), the surface heat transfer coefficient (h_f) is obtained (Eqn. 4). A list of temperature dependent (T_f) convective heat transfer coefficients (h_f) for natural convection on the conv₁ face (evaluated at surface temperature) is established for the purpose of the computational analysis and applied in ANSYS in [$^{\circ}\text{C}$] and offset by 273.15 [$^{\circ}\text{K}$]. The values of h_f vs T_f are presented in Figure 5.

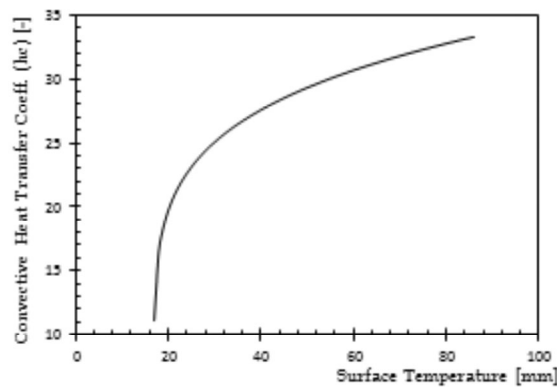


Figure 5: Convective Heat Transfer Coefficient (h_f) vs. Surface Temperature (T_s)

3.3 PHASE CHANGE

Plasticine is to be injected into the Gap Sachet in its liquid state and allowed to cool to a hardened solid state. Phase change transition initiates when the amplitude of the crystal lattice particles oscillate at a force having value larger than that of the crystal binding energy, thus breaking its bonds and transforming into liquid phase (melting). The removal of energy results in the solidification of the material (crystallization)[27].

The process of phase change during cooling exudes latent heat energy and is taken into account in ANSYS by employing the enthalpy model which defines the enthalpy as a function of temperature. The process is broken down into three phases, (1) solid phase (2) liquid phase and (3) mushy phase. Enthalpies are calculated for different temperature points, based on the latent heat energy dissipated, identifying the three stages detailed[28][29].

3.3.1 Determining Phase Change Enthalpies

Eqn. (2) details the three necessary properties required to be input into the governing equation for computation of a 3D thermal analysis, namely the density (ρ), specific heat capacity (c_p) and thermal conductivity (k). is the element specific heat matrix [J/kg-K] which is defined as:[10]

$$[C_e^t] = \int_{vol} \rho c \{N\} \{N\}^T .d(vol) \quad (12)$$

Where $\{N\}$ is the element shape function, defined as $N(x,y,z)$. The (ρc) terms in the equation above define the enthalpy (H , [J/m³]) through:

$$H = \int \rho c (T).dT \quad (13)$$

Thus for the enthalpy method, Eqn (13) is used to describe the relative value of enthalpy in the three states of plasticine (solid (H_s), mushy (H_m) and liquid (H_l)) with respect to temperature[30]:

$$H_s (T) = \int_{T_0}^{T_s} \rho c_{p(s)} (T).dT \quad (14)$$

$$H_m (T) = \int_{T_0}^{T_s} \rho c_{p(s)} (T).dT + \int_{T_s}^{T_l} \left\{ \rho \frac{H_L}{T_l - T_s} + \rho c_{p(m)} (T) \right\} .dT \quad (15)$$

$$H_l (T) = \int_{T_0}^{T_s} \rho c_{p(s)} (T).dT + \int_{T_s}^{T_l} \rho c_{p(m)} (T).dT + \int_{T_l}^T \rho c_{p(l)} (T).dT \quad (16)$$

Where T_s [°C] is the solidus temperature, T_0 [°C] is the lower limit reference temperature (taken to be 0 [°C]), T_l [°C] is the liquidus temperature, T_+ [°C] is the upper limit reference temperature (taken to be 90 [°C]), and $c_{p(m)}$ is the average of the solid and liquid specific heats. Eqn. (14) is applied within the temperature range ($T < T_s$), Eqn. (15) between ($T_s \leq T \leq T_l$) and Eqn. (16) between ($T > T_l$). Eqns. 14 to 16 are integrated [31][32] to obtain:

$$H_s = \rho c_{p(s)} (T_s - T_0) \quad (17)$$

$$H_m = H_s + \rho c_{p^{(*)}} (T_l - T_s) \tag{18}$$

$$H_l = H_m + \rho c_{p^{(l)}} (T_+ - T_l) \tag{19}$$

Where $c_p^{(*)}$ is defined as:

$$c_{p^{(*)}} = c_{p^{(m)}} + \frac{H_L}{T_l - T_s} \tag{20}$$

Eqns 17 to 19 can be used to define the enthalpy [J/m³] vs. temperature [°C] curve for the plasticine, after defining the limits of temperature.

3.3.2 Phase Change properties of Plasticine

Plasticine is a non-linear, viscoelastic, strain-rate softening/hardening material [33], whose exact composition is unknown, but is known to be composed primarily of calcium carbonate, paraffin wax and long-chain aliphatic acids. Due to the presence of paraffin wax, Plasticine is found to exhibit a phase change phenomenon which corresponds to the crystallization point of paraffin wax, allowing it flow in a liquid state beyond this temperature [34].

Due to the rheology of plasticine, it is commonly used as an analogue material to simulate deformation of geological structures[35], material flow in friction stir welding[36][37] and material forming processes[38][39][40]. The non-linear property of plasticine derives from structural changes in the material (through re-orientation of filler chains) and is reported to show softening beyond 200 [°K], similar to the glass transition phenomenon observed in glass [41]. The physical and thermal properties of plasticine is known to vary across the different brands, and also between the different colours it is manufactured in [35].

It is understood that in crystalline substances melting and solidification take place at the same temperature ($T_s = T_l = T_m$), typically assigned to be within 1 [°C] before the melting peak, while for amorphous substances the phase transition temperature is not located at one point, but takes place across a range of temperatures. ($T_s < T_m < T_l$) [42][43][31]. As such, a wide mushy zone is assigned, assuming $T_0 = 0$ [°C], $T_s = 24$ [°C], $T_l = 51$ [°C] and $T_+ = 90$ [°C].

A DSC analysis (Figure 6) on the plasticine yields $c_{p^{(s)}} = 1054$ [J/kgK] (at -24.98 °C), $c_{p^{(l)}} = 1456$ [J/kgK] (at 100.02 °C) and $H_L = 24,140$ [J/kgK] (at $T_m = 51.02$ °C). Eqns 17 to 20 are applied based on the fore-mentioned parameters, where the results are tabulated in Table 3, and the resulting Enthalpy vs. Temperature chart is shown in Figure 7.

Table 3: Enthalpy vs. Temperature (Eqn. 17 to 20)

Temperature [°C]	Enthalpy [J/m ³]
0.0	0
24.1	40,924,949
51	146,147,293
90	239,363,984

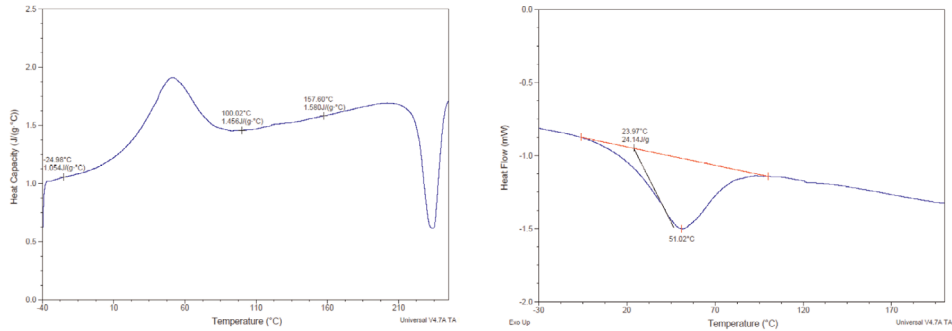


Figure 6: DSC Results of Plasticine

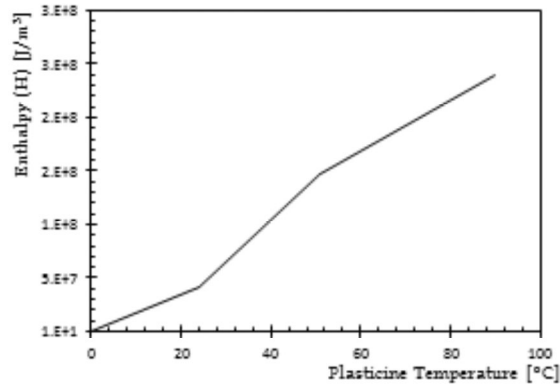


Figure 7: Enthalpy vs. Temp. Graph

3.4 THERMAL CONTACT CONDUCTANCE

When two nominally flat surfaces make contact, due to the microscopic irregularities on both surfaces contact is only made at a select number of discrete points. As a result, a temperature discontinuity exists at the mating interface where heat transfers not only through conduction at contact points, but also through convection and conduction of the fluid in the interstitial gaps, and radiation[5][44][45]. The Thermal Contact Conductance (TCC, h_c [W/m²-K]) is defined as:[46]

$$h_c = \frac{q}{\Delta T} \quad (21)$$

Where q [W/m²] is the heat flux (Q) per unit area (A) and ΔT [K] is the temperature drop at the mating interfaces. The value of h_c is dependent on parameters such as the surface roughness, hardness, interfacial pressure, thermal and physical material properties, and thickness [6].

Numerous methods exist to obtain experimentally and numerically, the value of thermal contact conductance between numerous interfaces among a for a wide range of the aforementioned parameters[45][47][48][49][50][51]. Results from [52] for tests conducted

on metal to polymer interfaces at ambient temperatures of 20 – 40 [°C] within a range of pressures (510 - 2760 KPa) yield thermal contact conductance values between 140.8 to 1659.4 [W/m²-K], where Nylon 6,6 has a range of thermal contact conductance between 366.5 – 447.4 [W/m²-K].

A parametric study will be conducted for the values of thermal contact conductance, by varying its value in the simulation through a range of 200 [W/m²-K] to 800 [W/m²-K] in steps of 200 [W/m²-K]. Temperature vs. time results for the Top and Bottom Plates will be compared to experimental data, where the curve which best represents the experimental temperature profile presents an accurate approximation of the value of thermal contact conductance.

It is assumed the value of thermal contact conductance are the same on both sides of the Gap Sachet's mating faces and that the faces are always in contact, from the point the Gap Sachet has been filled (static model). Further it is assumed that pure conduction from the plasticine into the plastic film takes place, and that the resistance due to heat flow is minimal as the plasticine is injected in its liquid state, thus being able to fill the space inside the Gap Sachet confidently, leading to perfect contact.

3.5 ESTIMATION OF INITIAL THERMAL LOADING

The initial temperature of plasticine is approximated based on experimental measurements at points T_1 and T_2 , after the injection is complete. The intermediate temperatures are derived using a linear extrapolation of temperatures between the aforementioned points, using:

$$T = mx + C \quad (22)$$

Where T [°C] is the temperature to be estimated at a point x [mm] along the length of the Gap Sachet, C is the y-intercept set as T_1 and m is the gradient obtained from:

$$m = \frac{T_2 - T_1}{30} \quad (23)$$

A total of 12 intervals (quadrants) are defined from the ranges of 0 [mm] to 30 [mm] at intervals of 2.5 mm. Eqn 22 is evaluated from x = 2.5 [mm] to x =27.5 [mm] and the results obtained (T [°C]) are used to define the temperatures within the respective quadrants. (Figure 4).

3.6 ANSYS TRANSIENT ANALYSIS

The simulation aims to portray in ANSYS, the transient thermal effects of the Gap Sachet during cooling. With the incorporation of Enthalpy (material non-linearity) and thermal contact conductance (contact non-linearity), the transient analysis becomes a non-linear one. The Newton-Raphson method of iteration is employed using the sparse solver to obtain converged results at every sub-step[43]. A summary of the time stepping regime is detailed in Table 4.

Table 4: Time Stepping Regime

Load Step Nr.	Start Time [s]	End Time [s]	Sub-Step Size [s]
#1	0	1.7	0.1
#2	1.7	20	0.1
#3	20	50	0.5

Using Eqns. 22 and 23, the estimated thermal loads are applied within the plasticine volume as a ramped load for Load Step #1, and is then removed in Load Step #2 & #3, simulating the thermal loads transferred from the plasticine during filling. The iteration convergence tolerance limit (TOLER) was set to the default number of 0.001, to be achieved by the 12th iteration. Minimum sub-step sizes of 0.1 [s] were found to produce converged and stable results[53][54].

The SmartSize meshing tool is used to mesh the four bodies created, using mesh setting of 5. For the purpose of the analyses SOLID70 elements (tetrahedral) were used. The incorporation of thermal contact conductance within the computational model involves the application of Target and Contact elements, defined through the Thermal Contact Wizard. TARGE170 and CONTA174 elements were used to define the 3D target and contact bodies (volumes). Figure 8 shows the 3D meshed model, comprising a total of 44,439 elements and 9,227 nodes respectively.

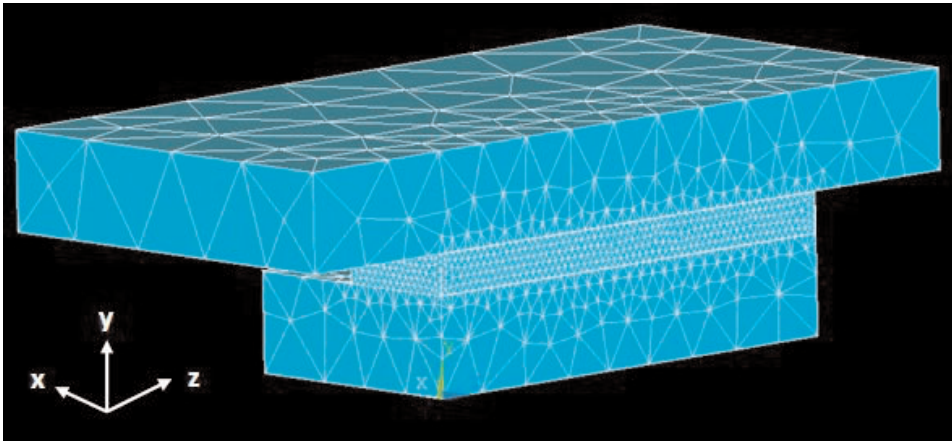


Figure 8: Meshed ANSYS model

4. RESULTS & DISCUSSION

Figure 9 show the results of the experimental measurements and computational analyses at points Top, Bottom, T_1 and T_2 for a range of thermal contact conductance values for $T_{injection} = 85$ [°C].

The Top, Bot and T_1 results show similarities with experimental results in terms of temperature profiles, with the exception of T_2 . As the injection hole has not been modelled on the $conv_1$ face, the plasticine within the Gap Sachet is not directly exposed to convection in the computational model, thus under predicting the drop in temperature after filling of the Gap Sachet has been completed at 1.7 seconds. Due to the low thermal conductivity of plasticine, this idealization does not manifest into large errors along the length of the Gap Sachet.

The initiation of phase change is seen at 51 [°C], characterised by a sharp change in slope of the temperature profile of T_1 and T_2 . Good agreement is seen for the curves of thermal contact conductance 400 [W/m-K] with experimental data indicating the true thermal contact conductance to be within this range. However due to the simplification of the Gap Sachet model the computational model maintains a larger volume of plasticine in comparison to the experiment and is therefore expected to over predict results. Further, the enthalpy model

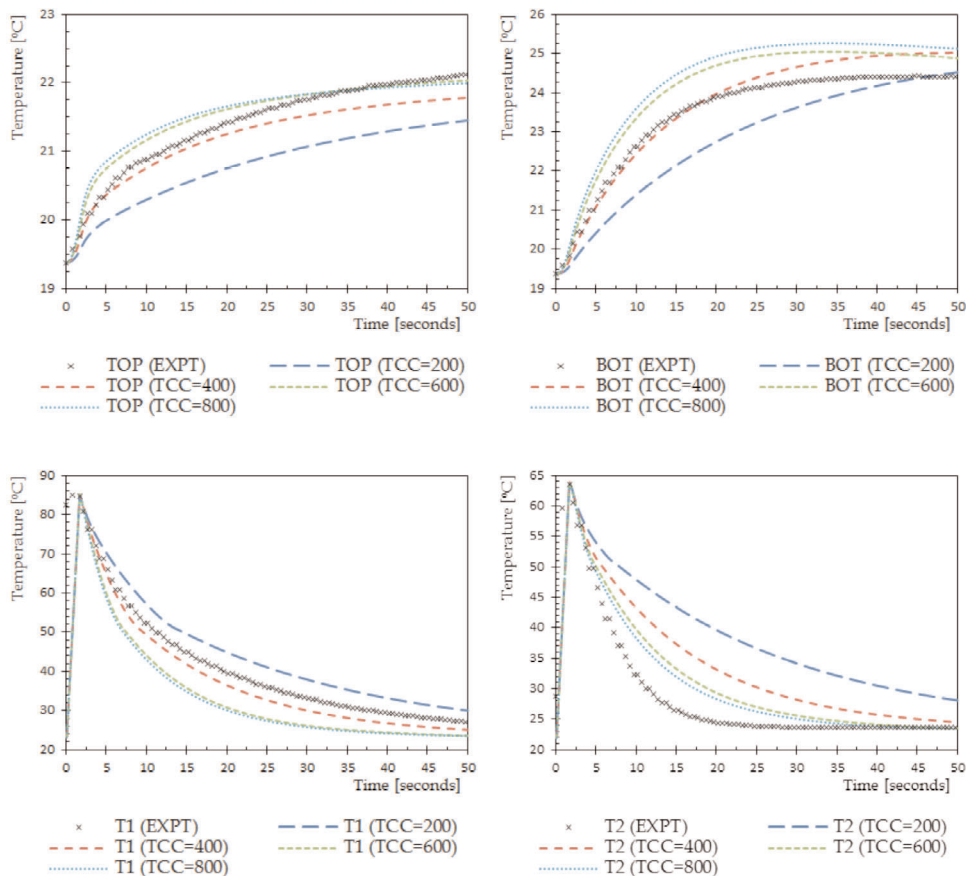


Figure 9: ANSYS Results; Temperature [°C] vs. Time [s] – Thermal Contact Conductance (TCC)

utilises the DSC results of melting curve for plasticine, where it is understood[55] that enthalpies of melting/fusion vary slightly in value and initiation and end temperatures, introducing further errors within the model.

Figure 10 shows the Nodal DOF temperature plots at different times for the thermal contact conductance value of 400 [W/m-K], where between $t = 0$ [s] to 1.7 [s], the linearly ramped thermal load can be seen to maintain the temperature distribution within the defined quadrants during the filling stage in the first Load Step. The subsequent images between $t = 5$ [s] to 50 [s] shows the cooling of the Gap Sachet in second and third Load Step. The conv₁ face is located on the right hand side of the figures.

Figure 11 shows the Nodal Flux Vector Sum at 1.7 seconds, where it can be seen the heat flux has initiated during the loading. At 10 seconds, the heat flux is seen on both top and bottom plates, with peaks located at corners of the Gap Sachet model. This idealization of the Gap Sachet model effectively increases the contact area between the top and bottom faces of the Gap Sachet, therefore the results of the heat flux are simply presented for a qualitative understanding of the flux field.

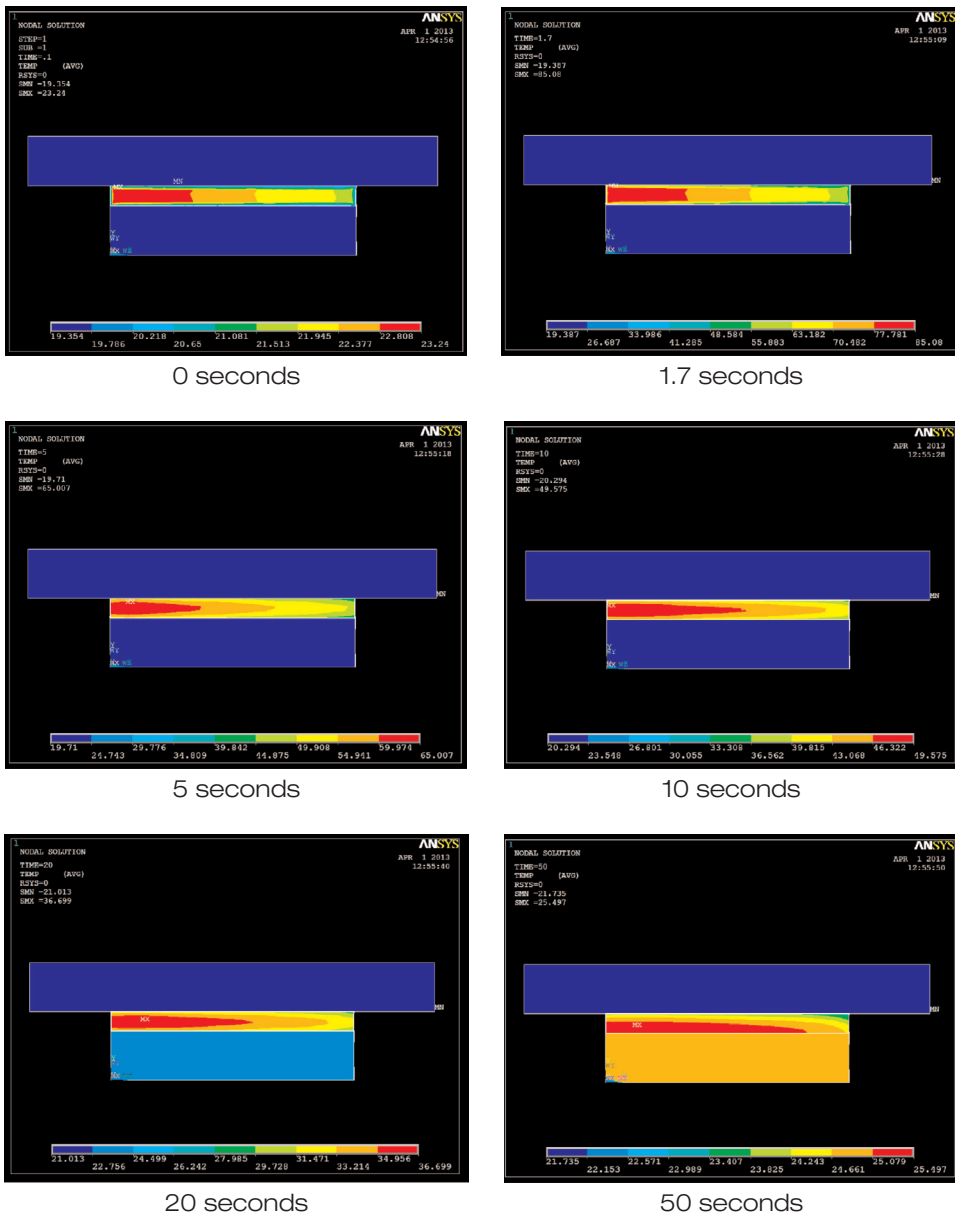


Figure 10: Nodal DOF Temperature plot at 0, 1.7, 5, 10, 20 and 50 seconds – TCC = 400 [W/m-K]

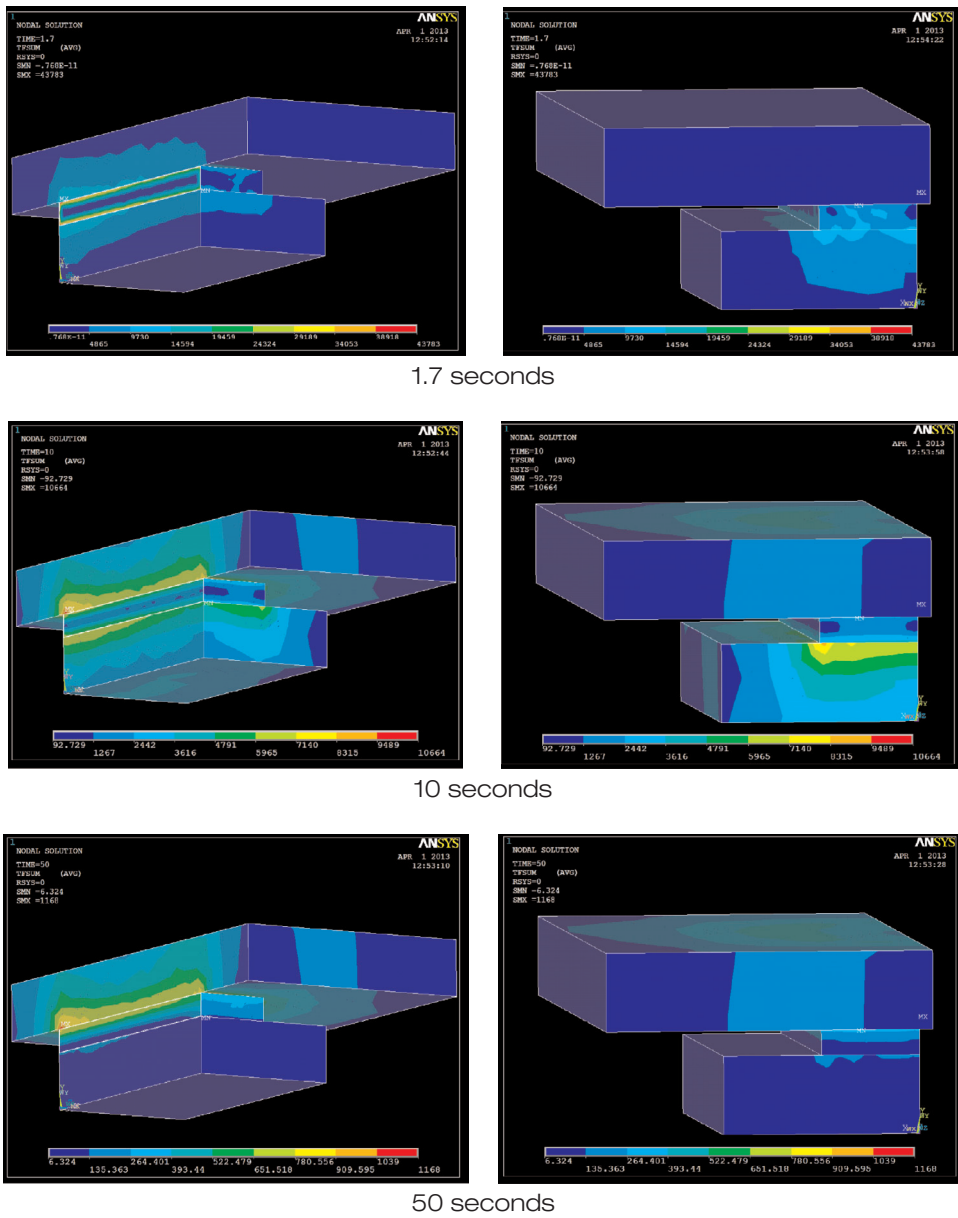


Figure 11: Nodal Flux Vector Sum plots at 1.7, 10 and 50 seconds – TCC = 400 [W/m-K]

5. CONCLUSION

The paper aimed to simulate the transient thermal processes involved during the cooling of the Gap Sachet when placed between two aluminium components. Phase change of plasticine was considered by applying the energy released during solidification over a wide mushy zone. Temperature dependent natural convection on one face was approximated and simulated through Nusselt number correlations, based on surface temperature. A parametric study was conducted on the value of Thermal Contact Conductance between the Gap Sachet and the adjacent contacting faces. Temperature vs. time profiles were shown to show good corroboration with experimental results, except for the exposed face, wherein the injection hole was not modelled, disallowing direct contact of the plasticine within the Gap Sachet with atmosphere. However, due to the low thermal conductivity of components of the Gap Sachet, the inaccuracy due to this simplification is observed to be minimal.

REFERENCES

- [1] S. Shan, L. Wang, T. Xin, Z. Bi. (2012). Developing a rapid response production system for aircraft manufacturing. *International Journal of Production Economics*.
- [2] Xiaobin, Y., (2008). GapSpace multi-dimensional assembly analysis. Ph. D. THE UNIVERSITY OF NORTH CAROLINA AT CHARLOTTE.
- [3] A.J. Comer, J.X. Dhôte, W.F. Stanley, T.M. Young. (2012). Thermo-mechanical fatigue analysis of liquid shim in mechanically fastened hybrid joints for aerospace applications. *Composite Structures*. 94 (7), p 2181-2187.
- [4] D'Apuzzo, N., (2006). Overview of 3D surface digitization technologies in Europe. *Proceedings- SPIE The International Society for Optical Engineering*. 6056 (0), p 605605 - 605606.
- [5] Syed M.S. Wahid, C.V. Madhusudana (2003) Thermal contact conductance: effect of overloading and load cycling, *International Journal of Heat and Mass Transfer*, Volume 46, Issue 21, Pages 4139-4143, ISSN 0017-9310
- [6] M. Rosochowska, R. Balendra, K. Chodnikiewicz. (2003). Measurements of thermal contact conductance. *Journal of Materials Processing Technology*. 135, p 204-210.
- [7] T M Kathryn. (2007). Considerations for Predicting Thermal Contact Resistance in ANSYS. *Proceedings of the 17th KOREA ANSYS User's Conference*
- [8] Lei Z., HongTae Kang, Yonggang Liu (2011) Finite Element Analysis for Transient Thermal Characteristics of Resistance Spot Welding Process with Three Sheets Assemblies, *Procedia Engineering*, Volume 16, 2011, Pages 622-631, ISSN 1877-7058
- [9] Aik Y. T., E.Schlecht, G. Chattopadhyay, R. Lin, C. Lee, J. Gill, I. Mehdi & J. Stake. (2011). Steady-State and Transient Thermal Analysis of High-Power Planar Schottky Diodes. *22nd International Symposium on Space Terahertz Technology*, p 26-28.
- [10] ANSYS (2009b). *Theory and Reference Guide*. USA: ANSYS
- [11] Kaiser K., (2009). Complete Thermal Design and Modeling for the Pressure Vessel of an Ocean Turbine – A Numerical Simulation and Optimization Approach. MSc. Florida Atlantic University, FL, USA
- [12] A. S. A. Elmaryami, B. Omar. (2012). Determination LHP of Axisymmetric Transient Molybdenum Steel-4037H Quenched in Sea Water by Developing 1-D Mathematical Model . *Metallurgical and Materials Transactions*. 18 (3), p 203-221.

- [13] A. Jafari, S.H. Seyedein & M. Haghpanahi. (2008). Modeling of Heat Transfer and Solidification of Droplet/Substrate in Microcasting SDM Process. *IUST International Journal of Engineering Science*. 19 (5-1), p 187-198.
- [14] N.Karunakaran and V.Balasubramanian . (2011). Multipurpose Three Dimensional Finite Element Procedure for Thermal Analysis in Pulsed Current Gas Tungsten Arc Welding of AZ 31B Magnesium Alloy Sheets. *International Journal of Aerospace and Mechanical Engineering*. 5 (4), p 267-274
- [15] Holdsworth, S. Daniel, Simpson, Ricardo (2008). *Thermal Processing of Packaged Foods*. 2nd ed. Springer. Chapter 2.
- [16] O. Ozsun, B E Alaca, A. D. Yalcinkaya, M. Yilmaz, M. Zervas and Y. Leblebici (2009). On heat transfer at microscale with implications for microactuator design. *Journal of Micromechanics and Microengineering*. 19 (4), p 1-13.
- [17] G. Su, Sugiyama Kenichiro, Yingwei Wu. (2007). Natural convection heat transfer of water in a horizontal circular gap. *Frontiers of Energy and Power Engineering in China*. 1 (2), p 167-173.
- [18] G.H. Su, Y.W. Wu, K. Sugiyama (2008) Natural convection heat transfer of water in a horizontal gap with downward-facing circular heated surface, *Applied Thermal Engineering*, Volume 28, Issues 11–12, August 2008, Pages 1405-1416, ISSN 1359-4311
- [19] A Ilgevicus (2004) Analytical and numerical analysis and simulation of heat transfer in electrical conductors and fuses, Ph.D, Universität der Bundeswehr München, Munich, Germany.
- [20] P. Juraj. (2012). *Cooling of an electric conductor by free convection – analytical, computational and experimental approaches*. Elektrotechnika, Strojárstvo .
- [21] F.J. McQuillan, J.R. Culham and M.M. Yovanovich. (1984). *Properties of Dry Air at One Atmosphere*. Microelectronics Heat Transfer Lab.
- [22] J. R. Lloyd & W. R. Moran. (1974). Natural Convection Adjacent to Horizontal Surface of Various Pianforms. *Journal of Heat Transfer*. 96, p 443 -447.
- [23] Goldstein, R. J., Sparrow, E. M., and Jones, D. C (1973) “Natural Convection, Mass Transfer-Adjacent to Horizontal Plates” *International Journal of Heat and Mass-Transfer*, Vol. 16, No. 5, May 1973, p. 1025-1034
- [24] A. Chandra and R. P. Chhabra. (2012). Effect of Prandtl Number on Natural Convection Heat Transfer from a Heated Semi-Circular Cylinder. *International Journal of Chemical and Biological Engineering*. 6, p. 69 - 75.
- [25] E. L. M. Padilla, R. Campregher, A. Silveira-Neto. (2006). Numerical Analysis of the Natural Convection in Horizontal Annuli at Low and Moderate RA. *Engenharia Térmica (Thermal Engineering)*. 5 (2), p. 58 - 65.
- [26] MASSIMO CORCIONE. (2008). Natural convection heat transfer above heated horizontal surfaces. *Int. Conf. on Heat and Mass transfer.*, p. 206 - 243.
- [27] Pavel Fiala, Ivo Behunek and Petr Drexler (2011). *Properties and Numerical Modeling-Simulation of Phase Changes Material*
- [28] P. Kopyt, M. Soltysiak, M. Celuch (2008) Technique for model calibration in retro-modelling approach to electric permittivity determination, *17th International Conference on Microwaves, Radar and Wireless Communications*

- [29] F. D. Bryant (2008). Modeling, Analysis and Experiment for Building Ice Parts with Supports Using Rapid Freeze Prototyping. *ProQuest*. p43.
- [30] Chen, L. Wang, P. L. Song, P. N. Zhang, J. Y.. (2007). Finite Element Numerical Simulation of Temperature Field in Metal Pattern Casting System and “Reverse Method” of Defining the Thermal Physical Coefficient. *ACTA Metallurgica Sinica*. 20 (3), p 217-224.
- [31] G. Feng, X. Sheng, Q. Chen, G. Li, H. Li. (2012). *Simulated analysis of the phase change energy storage kang heating and heat storage characteristics*. China Academic Journal
- [32] ANSYS (2009c) - Thermal Analysis Guide. USA: ANSYS
- [33] Janet Zulauf, Gernold Zulauf, Rheology of plasticine used as rock analogue: the impact of temperature, composition and strain, *Journal of Structural Geology*, Volume 26, Issue 4, April 2004, Pages 725-737, ISSN 0191-8141, 10.1016/j.jsg.2003.07.005.
- [34] Shouhu Xuan , Yanli Zhang , Yufeng Zhou , Wanquan Jiang and Xinglong Gong. (2012). Magnetic Plasticine™: a versatile magnetorheological material. *Journal of Materials Chemistry*. 22, p 13395 - 13400.
- [35] Martin P.J. Schöpfer, Gernold Zulauf (2002) Strain-dependent rheology and the memory of plasticine, *Tectonophysics*, Volume 354, Issues 1–2, 30 August 2002, Pages 85-99, ISSN 0040-1951
- [36] B.C. Liechty, B.W. Webb, (2007b) Flow field characterization of friction stir processing using a particle-grid method, *Journal of Materials Processing Technology*, Volume 208, Issues 1–3, 21
- [37] B.C. Liechty, B.W. Webb (2007c) The use of plasticine as an analog to explore material flow in friction stir welding, *Journal of Materials Processing Technology*, Volume 184, Issues 1–3, 12 April 2007, Pages 240-250, ISSN 0924-0136
- [38] K Eckerson, B Liechty, C D Sorensen. (2008). Thermomechanical similarity between Van Aken plasticine and metals in hot-forming. *The Journal of Strain Analysis for Engineering Design*. 43 (5), p 383 - 394.
- [39] Geunan Lee, Eundeog Chu, Yong-Taek Im, Jongsoo Lee (1993) AN EXPERIMENTAL STUDY ON FORMING AXI-SYMMETRIC HEAVY FORGING PRODUCTS USING MODELLING MATERIAL, In: W.B. Lee, Editor(s), *Advances in Engineering Plasticity and its Applications*, Elsevier, Oxford, 1993, Pages 917-922, ISBN 9780444899910
- [40] K Eckerson, B Liechty, C D Sorensen. (2008). Thermomechanical similarity between Van Aken plasticine and metals in hot-forming. *The Journal of Strain Analysis for Engineering Design*. 43 (5), p 383 - 394.
- [41] Hui Ji, Eric Robin, Tanguy Rouxel (2009) Compressive creep and indentation behavior of plasticine between 103 and 353K, *Mechanics of Materials*, Volume 41, Issue 3, March 2009, Pages 199-209, ISSN 0167-6636
- [42] Pavel Fiala, Ivo Behunek and Petr Drexler (2011). *Properties and Numerical Modeling-Simulation of Phase Changes Material, Convection and Conduction Heat Transfer*, Dr. Amimul Ahsan (Ed.), ISBN: 978-953-307-582-2, InTech, Available from: <http://www.intechopen.com/books/convection-and-conduction-heattransfer/properties-and-numerical-modeling-simulation-of-phase-changes-material>

- [43] M. M. Pariona, A. C. Mossi (2005). Numerical Simulation of Heat Transfer During the Solidification of Pure Iron in Sand and Mullite Molds. *Journal of the Brazilian Society of Mechanical Sciences*. XXVII (4), 339 - 406.
- [44] Ravi Prasher. (2006). Thermal Interface Materials: Historical Perspective, Status, and Future Directions. *Proceedings of the IEEE*. 94 (8), 1571 - 1586.
- [45] G. P. Peterson and L. S. Fletcher. (1988). Evaluation of Thermal Contact Conductance Between Mold Compound and Heat Spreader Materials. *Journal of Heat Transfer*. 110, 996 - 998.
- [46] C.V. Madhusudana (1996) *Thermal Contact Conductance*, Springer, Berlin. ISBN 0-387-94534-2
- [47] K. C. Toh and K. K. Ng. (1997). Thermal Contact Conductance of Typical Interfaces in Electronic Packages Under Low Contact Pressures. *IEECPMT Electronic Packaging Technology Conference*. p 130-135
- [48] G. P. Peterson, L. S. Fletcher. (1988). Thermal Contact Conductance of Packed Beds in Contact With a Flat Surface. *Journal of Heat Transfer*. 110 (37), 38 - 41.
- [49] S. R. Mirmira, E. E. Marotta, and L. S. Fletcher. (1997). Thermal Contact Conductance of Adhesives for Microelectronic Systems. *Journal of Thermophysics and Heat Transfer*. 11 (2), 141 – 145
- [50] J. J. Fuller and E. E. Marotta. (2001). Thermal Contact Conductance of Metal/Polymer Joints: An Analytical and Experimental Investigation. *Journal of Thermophysics and Heat Transfer*. 15 (2), 228 - 238.
- [51] M. Bahrami, M. M. Yovanovich, E. E. Marotta. (2006). Thermal Joint Resistance of Polymer-Metal Rough Interfaces. *Journal of Electronic Packaging*. 128, 23 - 29.
- [52] E. E. Marotta and L. S. Fletcher. (1996). Thermal Contact Conductance of Selected Polymeric Materials. *Journal of Thermophysics and Heat Transfer*. 10 (2), 334 - 342.
- [53] Mayboudi, L, S (2008). Heat Transfer Modelling and Thermal Imaging Experiments in Laser Transmission Welding of Thermoplastics. Ph. D. Queen's University, Canada (ON)
- [54] Roger Stout, P.E. David Billings, P.E. (2002). *Accuracy and Time Resolution in Thermal Transient Finite Element Analysis*
- [55] B.L. Gowreesunker, S.A. Tassou, M. Kolokotroni (2012) Improved simulation of phase change processes in applications where conduction is the dominant heat transfer mode, *Energy and Buildings*, Volume 47, April 2012, Pages 353-35
- [56] Powell, R.W. Ho, C.Y., Liley, P.E (1966). *Thermal conductivity of selected materials* (United States National Standard Reference Data Series, 8), p27
- [57] Cobden, R., Alcan, Banbury (1994): Physical Properties, Characteristics and Alloys (EAA - European Aluminium Association)
- [58] Sommer, J. L. (1997) *High Conductivity, Low Cost Aluminum Composite for Thermal Management*
- [59] Holly M. V.. (2012). Material Properties: Polyamide (Nylon). Available: [http://cryogenics.nist.gov/MPropsMAY/Polyamide%20\(Nylon\)/PolyamideNylon_rev.htm](http://cryogenics.nist.gov/MPropsMAY/Polyamide%20(Nylon)/PolyamideNylon_rev.htm). Last accessed 2nd April 2013.
- [60] Airtech (2013). Iplon KM1300 DATA SHEET

